Science of the Total Environment 901 (2023) 166490

Contents lists available at ScienceDirect

Science of the Total Environment

journal homepage: www.elsevier.com/locate/scitotenv

Urbanization expands the fluctuating difference in gross primary productivity between urban and rural areas from 2000 to 2018 in China

Xiaoyan Liu [a,b,c,f], Yaoping Cui [a,b,c,f,*], Wanlong Li [a,b], Mengdi Li [a,b], Nan Li [a,b], Zhifang Shi [a,b], Jinwei Dong [d], Xiangming Xiao [e,**]

[a] *Key Laboratory of Geospatial Technology for the Middle and Lower Yellow River Regions (Henan University), Ministry of Education, Kaifeng 475001, Henan, China*
[b] *School of Geography and Environmental Science, Henan University, Kaifeng 475004, China*
[c] *Dabieshan National Observation and Research Field Station of Forest Ecosystem at Henan, Zhengzhou 450046, China*
[d] *Institute of Geographical Sciences and Resources, Chinese Academy of Sciences, Beijing 100101, China*
[e] *Department of Microbiology and Plant Biology, Center for Earth Observation and Modeling, University of Oklahoma, Norman, OK 73019, USA*
[f] *Xinyang Ecological Research Institute, Xinyang 464000, China*

HIGHLIGHTS

- GPP in 34 main cities in China increased with urbanization.
- The upward trend of urban GPP was greater than for rural GPP.
- Steady fluctuation in urban GPP implies the toughness of urban environment for vegetation growth.
- Contribution of human activities to GPP in UA and RA was 51 % and 24 %, respectively.
- The decreased GPP in UA was partly compensated by the growth offset of urbanization.

GRAPHICAL ABSTRACT

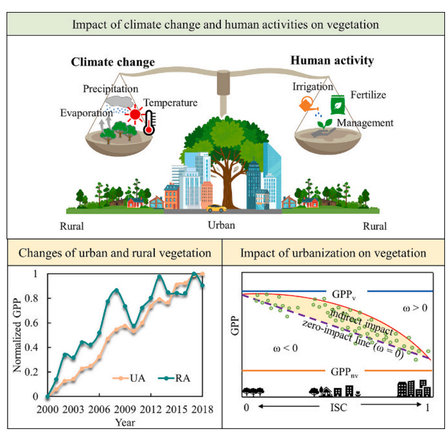

ARTICLE INFO

Editor: Shuqing Zhao

Keywords:
Urbanization
Gross primary productivity
Climate change
Human activity
Growth offset

ABSTRACT

Urban and rural vegetation are affected by both climate change and human activities, but the role of urbanization in vegetation productivity is unclear given the dual impacts. Here, we delineated urban area (UA) and rural area (RA), quantified the relative impacts of climate change and human activities on gross primary production (GPP) in 34 major cities (MCs) in China from 2000 to 2018, and analyzed the intrinsic impacts of urbanization on GPP. First, we found that the total urban impervious surface coverage (ISC) of the 34 MCs increased by 13.25 % and the mean annual GPP increased by 211 gC m^{-2} during the study period. GPP increased significantly in urban core areas, but decreased significantly in urban expansion areas, which was mainly due to a large amount of

* Correspondence to: Y. Cui, Key Laboratory of Geospatial Technology for the Middle and Lower Yellow River Regions (Henan University), Ministry of Education, Kaifeng 475001, Henan, China.
** Corresponding author.
E-mail addresses: cuiyp@lreis.ac.cn (Y. Cui), xiangming.xiao@ou.edu (X. Xiao).

https://doi.org/10.1016/j.scitotenv.2023.166490
Received 21 May 2023; Received in revised form 16 August 2023; Accepted 20 August 2023
Available online 21 August 2023

vegetation loss due to land use conversion. Second, the variability of GPP in UA was generally lower than in RA. Both climate change and human activities had a positive impact on GPP in UA and RA in the 34 MCs, of which the contribution was 49 % and 51 % in UA, and 76 % and 24 % in RA, respectively. Third, under climate change and human activities, the increase in GPP offset 4.96 % and 12.35 % of the impact of land use conversion on GPP in 2000 and 2018, respectively, which indicated that the offset strengthened over time. These findings emphasize the role of human activities in promoting carbon sequestration in urban vegetation, which is crucial for better understanding the processes and mechanisms of urban carbon cycles. Decision-makers can manage urban vegetation based on vegetation carbon sequestration potential as regions urbanize, aiding comprehensive decision-making.

1. Introduction

Cities have always been the hot spots that lead to regional environmental changes (Grimm et al., 2008). About 55 % of the global population lives in cities, and more than half of economic activities take place in cities in 2017 (Ritchie and Roser, 2018). Rapid urbanization changes the regional climate and human activities, and thus affects the growth environment of urban vegetation (Grimm et al., 2008; Ou et al., 2013; Tan et al., 2018). The environment in cities is affected by climate change and human activities, and cities have become natural laboratories for studying the relationship between climate change and vegetation (Zhang et al., 2022; Zhao et al., 2016). Thus, investigating the impact of the urban environment on vegetation growth is important for advancing our knowledge of the potential response of vegetation to climate change and human activities.

Vegetation growth is driven by both climate change and human activities, and their impacts can be positive or negative (Zheng et al., 2019; Xie et al., 2020). An important condition that impacts the distribution of vegetation is climate, which determines the temperature, sunlight, and water conditions that plants experience. Some studies showed that the temperature will continue to increase in the future, which will prolong the vegetation growing season and affect urban vegetation productivity (Ahlström et al., 2012; Khon et al., 2007; Walker et al., 2015). However, high air temperatures might inhibit the carbon sequestration capacity of vegetation (Liu et al., 2018c). Furthermore, the spatial variation of gross primary production (GPP) can also be explained by either precipitation or evapotranspiration (Shi et al., 2021; Garbulsky et al., 2010). Among them, actual evapotranspiration can be considered as a proxy for net primary productivity, because actual evapotranspiration represents the simultaneous availability of vegetation energy and water by vegetation (Lutz et al., 2010). In addition, human activities have been proven to be an extremely important factor that influences vegetation growth (Jiang et al., 2017b; Ge et al., 2021; Tang et al., 2020). Vegetation in cities often has comprehensive management and planning strategies, including irrigation, green belt construction, and urban landscape design. Thus, urban vegetation has human-dominated recessive features and different characteristics in vegetation growth (Zhao et al., 2012; Miller et al., 2018). Thus, understanding the impacts of climate change and human activities on vegetation is crucial for developing adaptation strategies to address the challenges that both pose to the ecosystems (Jiang et al., 2017a).

Most of the previous studies focused on the impacts of climate change and human activities on regional vegetation, but in urban areas, especially in areas with rapid urbanization processes, the extent to which vegetation growth is impacted by climate change and human activities is not clear. Therefore, it is important to quantify and compare the impacts of urban management and climate (UMC) on vegetation growth in urban and rural areas (Zheng et al., 2019; Huang et al., 2020; Liu et al., 2022).

Generally, the reduction of vegetation area due to land use transformation caused by urbanization is a direct negative impact, but some studies have found that urbanization has indirect impacts on vegetation that can be positive or negative (Tian and Qiao, 2014; Liu et al., 2018b; Liu et al., 2019; Cui et al., 2022; Sun et al., 2020; Chen et al., 2021a, 2021b). The indirect impact of urbanization on vegetation is increasingly being explored and recognized in recent years (Cui et al., 2022; Zhong et al., 2019; Zhao et al., 2016; Watts, 2017; Velasco et al., 2016). Using vegetation indices (VIs), some studies confirmed that there can be positive impacts of urbanization on vegetation growth in urban areas in China and even around the world (Zhao et al., 2016; Zhu et al., 2016; Cui et al., 2022).

GPP is the total amount of organic carbon fixed by photosynthesis, which plays a key role in measuring and monitoring vegetation growth (Anav et al., 2015; Liu et al., 2018b; Nuarsa et al., 2018). While GPP has been utilized for analyzing the influence of urbanization on vegetation within a specific city, it is important to acknowledge the substantial variations in both climatic conditions and the level of urbanization across different regions in China (Zhong et al., 2019). Thus, when considering the broader scope of climate change and human activities, studying the impact of urbanization on vegetation and carbon sequestration can provide insights into the intrinsic impact of the urban environment on vegetation. It helps determine whether this impact follows a universal pattern or exhibits regional variations.

China has experienced unprecedented rapid urbanization, and municipalities and provincial capitals are important centers of China's society and economy. These rapidly developing urban areas are particularly useful for exploring the impact of China's urbanization on vegetation. Using long-term GPP, impervious surface (IS), and climate data, including temperature, precipitation, reference evapotranspiration and actual evapotranspiration, we aimed to (1) evaluate the differences in the contributions of climate change and human activities to urban and rural GPP in 34 major cities (MCs) in China, and (2) quantify the impact of urbanization on vegetation productivity. This study aims to evaluate the alterations in vegetation carbon sequestration capacity throughout the process of urbanization in China, as well as its impact on this capacity. Moreover, we will elucidate the disparities in vegetation carbon sequestration capacity changes between urban and rural areas, emphasizing the suitability of urban environments for effective vegetation carbon sequestration.

2. Materials and methods

2.1. Study area

China has four municipalities, 23 provinces, five autonomous regions, two special administrative regions, and a total of 34 major cities (MCs). The topographical heights of the 34 MCs are ununiform. Most of the cities are in the central, eastern, and coastal areas of China, with flat terrain and elevations below 2000 m. Since the impervious surface in the administrative areas that correspond to Lhasa and Chongqing are mainly distributed in the center of the city, we selected Duilong Deqing County, Chengguan District, and Dazi District in Lhasa and 16 districts in Chongqing for study. The 34 MCs and their surrounding urban agglomerations (such as the Yangtze River Delta, Pearl River Delta, and Beijing-Tianjin-Hebei) have become the main sources of China's economic growth. As of 2018, China had a population of 1.405 billion and a GDP of 91.93 trillion yuan. Municipalities and provincial capitals had a population of 318 million or 21.17 % of China's total, and 34.74 % of

China's GDP (China Economic and Social Big Data: https://data.cnki.net/) (Table S1 Supplementary Material). We utilized the Methods S1 in Supplementary Material to accurately define the urban and rural area boundaries, enabling us to analyze and quantify the difference fluctuations of GPP between urban and rural areas (UA and RA) (Methods S1) (Fig. 1).

2.2. Data

2.2.1. Impervious surface coverage (ISC) data

Fine-scale impervious surface data plays a crucial role in monitoring the progression of urbanization and land use conversion, while also providing valuable insights into the extent of the transition from natural landscapes to impervious areas (Yang et al., 2019). In recent years, Gong et al. (2020) employed the Google Earth Engine (GEE) platform to generate the global artificial impervious areas (GAIA) dataset. This dataset spans from 1985 to 2018 and was constructed using Landsat satellite images with a horizontal resolution of 30 m (obtained from http://data.ess.tsinghua.edu.cn), nighttime light data, and Sentinel-1 radar data as auxiliary information. The improved algorithm utilized by Gong et al. (2020) effectively distinguished impervious surfaces from bare ground, resulting in an overall mean accuracy of over 90 % (Gong et al., 2020; Zhang et al., 2022). Consequently, the GAIA dataset has become a widely used resource for analyzing urbanization. In our study, we utilized the GAIA dataset to examine urbanization development. Moreover, to ensure compatibility with the spatial resolution of the GPP data, we aggregated the GAIA data and calculated the percent impervious surface coverage (ISC) within each 500 m grid cell. This metric ranges from 0, representing full vegetation, to 100 %, indicating complete impervious surface coverage.

2.2.2. Gross primary production (GPP) of vegetation data

The GPP data utilized in this study was originally developed by Zhang et al. (2017), who used an improved LUE theory and developed a new global Vegetation Photosynthesis Model (VPM) dataset that included GPP for all land areas, including urban and rural areas. This provides a product for analyzing the differences in vegetation productivity between urban and rural areas in this study (Zhang et al., 2017). To further validate the reliability of the GPP data in urban areas, several scholars have conducted assessments by comparing it with solar-induced chlorophyll fluorescence (SIF) data. Noteworthy studies by Cui et al. (2017), Ma et al. (2018), and Doughty et al. (2021) have affirmed the effectiveness of this dataset in accurately reflecting vegetation productivity in urban environments. The spatial resolution of GPP dataset was 500 m, the temporal resolution was 8 days, and the unit was $gC\,m^{-2}\,day^{-1}$. To enhance the usability of the 8-day GPP, we employed a Savitzky–Golay filter for smoothing as detailed in Supplementary Method file S2. Additionally, we aggregated the GPP data from 2000 to 2018 to generate annual GPP products (Chen et al., 2004; Fontana et al., 2008).

2.2.3. Climate data

Accurate and high-resolution climatic data is of paramount essential for various ecological applications. In our study, we obtained the surface air temperature (*T*) and precipitation (*PR*) form the Climatologies at high resolution for the earth's land surface areas (CHELSA) dataset, including high spatial and temporal resolution from 2000 to 2018 (Karger et al., 2017). *T* is mainly based on the monthly means in K of daily mean temperature obtained from the six-hour synoptic data from the European Centre for Medium-Range Weather Forecast (ECMWF) climatic reanalysis interim (ERA-Interim). *PR* combines topographic factors, including wind fields, valleys, and boundary layer heights where airflow interacts with topography and uses methods such as bias correction to obtain monthly precipitation, in mm. Furthermore, on a global scale, the coefficient between CELSA temperature and MOD11C3 ranged from 0.95 to 0.99, and compared to precipitation in WorldClim, *PR* captured terrain inhomogeneity well at medium and small scales (Karger et al., 2017). The spatial resolution was 30 arcseconds. In addition to the CHELSA dataset, the reference evapotranspiration (ET_0) and actual evapotranspiration (*AET*) datasets in this study are mainly obtained from the TerraClimate dataset on the GEE platform (Abatzoglou et al., 2018). The TerraClimate dataset is a comprehensive monthly climate balance dataset that covers the global land surface. It provides accurate and extensive climate data on a global scale, making it a valuable resource for analyzing regional and even global climate change characteristics (Berner and Goetz, 2022; Hammond et al., 2022; Li et al., 2023). ET_0 is calculated based on a measure of potential moisture loss, using the Penman-Monteith equation, which is not a purely temperature-based measure but uses an energy balance approach to estimate potential evapotranspiration. *AET* is calculated based on the one-dimensional soil water balance model, accounting for interactions between precipitation, ET_0, and soil and snowpack water storage (Abatzoglou et al., 2018). The spatial resolution of the ET_0 and *AET* datasets are approximately 1/24°, and their units are mm. To account for the impact of climatic factors on vegetation growth, the *T*, *PR*, ET_0, and *AET* datasets were projected and then resampled through a bilinear interpolation method to match the geographic coordinate system and spatial resolution of the GPP dataset.

2.3. Methods

2.3.1. Adjacent-varying fluctuations F_σ and F_s

The adjacent-varying fluctuations can inform the fluctuations of GPP in adjacent years, and reflect the stability of the corresponding parameters. Combining the standard deviation and the coefficient of variation, we utilized a method that can quantify the fluctuation of the data in adjacent years, namely adjacent-varying fluctuations. F_σ and F_s were used to reflect the degree and magnitude of the adjacent-varying fluctuation of the data. We assumed that regions with small fluctuations provide a more tough or suitable environment for vegetation growth. The specific workflow is as follows:

(1) Normalize the data with dimensions or large-scale differences into a dimensionless form as a scalar. To ensure the comparability and reliability of the results, it is crucial to standardize the variables by converting them into dimensionless quantities before analyzing the data. This process eliminates the impact of differing attributes, enabling a unified standard of comparison. By removing these variations, the results become more robust and facilitate meaningful comparisons. (Eq. (1)):

$$N_i = \frac{A_i - A_{min}}{A_{max} - A_{min}} \tag{1}$$

where i= 1, 2, 3, …, n. $A_i$is the i_{th} year of a group of data. N_i was the result of A_i normalization processing. A_{min} and A_{max} are the minimum and maximum values of this group of data, respectively.

(2) Count the changes in the data of adjacent years. In time series analysis, a common method to examine statistical changes in the data between adjacent years is by calculating the difference between them. This approach allows for a comprehensive understanding of the variations occurring over time (Eq. (2)):

$$m_i = N_{i+1} - N_i \tag{2}$$

where m_i is the change value in two adjacent years.

(3) Calculate the adjacent-varying fluctuations F_σ and F_s. Standard deviation is an indicator used to reflect the degree of concentration of data, represented by σ (Methods S4). The calculation of the standard deviation of m_i (F_σ) is a valuable metric for assessing the fluctuation of data over time. By analyzing the standard

Fig. 1. Spatial distribution of the 34 major Chinese cities.

deviation, we gain a clearer understanding of the level of volatility or stability present in the data over the given time period. F_s is a summary of data changes over time. It provides a valuable measure of the overall amount of data variation occurring within a given timeframe. (Eq. (3) and Eq. (4)):

$$F_{\sigma} = \sqrt{\frac{1}{n-1}\sum_{i=1}^{n-1}\left(m_i - \frac{1}{n-1}\sum_{i=1}^{n-1} m_i\right)^2} \tag{3}$$

$$F_s = \sum_{i=1}^{n-1}|m_i| \tag{4}$$

where the smaller the value of the adjacent-varying fluctuations F_{σ} and F_s, the more stable the data.

2.3.2. Screen the main climate impact factors

We simulate the vegetation response to climate change based on four climate factors: T, PR, ET_0, and AET. However, changes in one climate factor inevitably affect the variations of other factors, and the relationships among these factors are also complex. Therefore, to ensure the representativeness and accuracy of the established multiple regression model, while controlling the influence of other related climatic factors, this study analyzes the degree of partial correlation between the four climate factors and GPP based on partial correlation coefficients $r_{x\cdot GPP}$ (Eq. (5)), identifying the climate factors with strong correlations in each MC (Gu et al., 2018; Wu et al., 2015).

$$r^2{}_{1\cdot n} = \frac{R^2{}_{1(2,3,\ldots,n)} - R^2{}_{1(3,\ldots,n)}}{1 - R^2{}_{1(3,\ldots,n)}} \tag{5}$$

where n represents how many variables there are; $r^2{}_{1\cdot n}$ refers to the partial correlation coefficient between 1 and n; $R^2{}_{1(2,3,\ldots,n)}$ represents the coefficient of determination for the regression analysis of variable 1 with variables (2, 3, …, n); $R^2{}_{1(3,\ldots,n)}$ represents the coefficient of determination for the regression analysis of variable 1 with variables (3, …, n). For instance, in this study, there are five variables: T, PR, ET_0, AET, and GPP. The partial correlation coefficient, $r_{T\cdot GPP}$, indicates the correlation between GPP and T under the conditions of fixed PR, ET_0, and AET, and the same applies in reverse.

2.3.3. Quantifying the contributions of climate change and human activities to GPP

The growth of vegetation is influenced by a combination of climate change and human activities. In this study, we employed multiple linear regression residual analysis to assess the contributions of climate change and human activities on vegetation GPP. Specific steps were as follows (Shi et al., 2021):

(1) We used the monthly mean GPP as the dependent variable and each climate factor as the independent variable and established multiple linear regression models and calculated the parameters.
(2) We computed the predicted value of gross primary productivity (GPP_{CC}) by establishing a regression relationship model between climatic conditions and observed GPP (GPP_{CC}). This model enabled us to isolate the specific contribution of climate change to GPP (Eq. (6)).
(3) The difference between the predicted value (GPP_{CC}) and the actual value (GPP_{obs}) was the residual (Evans and Geerken, 2004), that is, the impact of human activities on GPP (GPP_{HA}) (Eq. (7)):

$$GPP_{CC} = \beta_0 + \beta_1 x_1 + \beta_2 x_2 + \cdots + \beta_n x_n \tag{6}$$

$$GPP_{HA} = GPP_{obs} - GPP_{CC} \tag{7}$$

where β_0, β_1, …, β_n are parameters, x_1, x_2, …, x_n are the monthly mean climate factors from March to November: T, PR, ET_0, and AET.

According to the $Slope$ trend analysis of Methods S3, $Slope_{pre}$ and $Slope_{res}$ represent the trend of GPP_{CC} and GPP_{HA} from 2000 to 2018, respectively ((Eq. (8) and Eq. (9)):

$$Slope_{pre} = \frac{19 \times \sum_{i=1}^{19}(i \times GPPpre_i) - \sum_{i=1}^{n} i \times \sum_{i=1}^{n} GPPpre_i}{19 \times \sum_{i=1}^{19} i^2 - \left(\sum_{i=1}^{19} i\right)^2} \tag{8}$$

$$Slope_{res} = \frac{19 \times \sum_{i=1}^{19}(i \times GPPres_i) - \sum_{i=1}^{n} i \times \sum_{i=1}^{n} GPPres_i}{19 \times \sum_{i=1}^{19} i^2 - \left(\sum_{i=1}^{19} i\right)^2} \tag{9}$$

where i is the sequential year range (2000–2018).

$Slope_{pre}$ and $Slope_{res}$ quantified the degree to which climate change and human activities promoted (if $Slope > 0$) or inhibited (if $Slope < 0$) GPP (Table S2). Furthermore, according to the method proposed by Sun et al. (2015), the contributions of climate change and human activities to GPP were obtained separately (Table S3) (Sun et al., 2015).

2.3.4. Quantifying the intrinsic impact of urbanization on GPP

There are some limitations in quantifying the contribution of climate change and human activities to GPP based on the trend of GPP from 2000 to 2018. Strictly speaking, it cannot reveal the inherent impact of urbanization on GPP, especially the impact of land use conversion and UMC. Therefore, to systematically quantify the impact of urbanization on vegetation growth, we drew on the theoretical framework proposed by Zhao et al. (2016) that urban GPP can be decomposed into the contributions of vegetation and non-vegetation (Zhao et al., 2016). The zero-impact line is defined by full vegetation and full ISC, representing the condition under which urbanization does not impact GPP ($\omega_i = 0$) (Eq. (10)):

$$GPP_{zi} = (1 - ISC) \times GPP_v + ISC \times GPP_{nv} \tag{10}$$

where GPP_{zi} is the GPP only affected by ISC, GPP_v is the GPP corresponding to full vegetation ($ISC = 0$, $GPP = GPP_v$), and GPP_{nv} is the GPP corresponding to full ISC ($ISC = 1$, $GPP = GPP_{nv}$) (Fig. S1 Supplementary Material).

Urbanization can alter vegetation growth, and its impact of climate change and human activities on the vegetation is indirect, which contrasts with the direct impact of land use conversion. The indirect impact ω_i can be measured by the relative change in GPP_{obs} to the zero-impact line (Eq. (11)):

$$\omega_i = \frac{GPP_{obs} - GPP_{zi}}{GPP_{zi}} \times 100\% \tag{11}$$

where GPP_{obs} is the observed GPP of the pixel. Comparing the indirect effect of urbanization on GPP ($GPP_{obs} - GPP_{zi}$) with the direct impact of GPP loss from land use conversion ($GPP_v - GPP_{zi}$) as a growth offset τ (Eq. (12)):

$$\tau_i = \frac{GPP_{obs} - GPP_{zi}}{GPP_v - GPP_{zi}} \times 100\% \tag{12}$$

A positive τ indicates that urbanization promotes vegetation growth, i.e., the direct negative impact of urbanization ($GPP_v - GPP_{zi}$) is offset to some extent by the indirect positive impact. Conversely, if τ is negative, urbanization will exacerbate the immediate negative impact.

3. Results

3.1. Spatial-temporal changes of ISC and GPP in UA and RA

Urbanization continued to develop in China from 2000 to 2018. The area of UA increased from 10,880 km^2 in 2000 to 40,726 km^2 in 2018 in 34 MCs, with a mean growth of 1803 km^2 yr^{-1} (Fig. S2). In 2018, the area of UA increased by more than double in 86 % of the 34 MCs (Table S4). The mean ISC increased from 17.73 % in 2000 to 30.98 % in

2018. Of all grid cells, 91.08 % (514,093 grid cells) had a significant upward trend, with a mean growth rate of 1.28 % yr^{-1} (Fig. S3a). Of the 34 MCs, 67 % had a higher mean ISC (24.03 %), which were mainly in the Beijing-Tianjin-Hebei region, the Central Plains, and the Yangtze River Delta (Table S5 and Fig. 2).

On the whole, GPP had a fluctuating upward trend from 2000 to 2018, with a mean GPP of 1092 gC m^{-2} yr^{-1}. The mean GPP increased from 935 gC m^{-2} yr^{-1} in 2000 to 1146 gC m^{-2} yr^{-1} in 2018, and 91 % of the 34 MCs had an upward trend. However, Shanghai, Nanjing, and Xining had downward trends in GPP (Fig. S3b). The spatial distribution of GPP was uneven, in which the mean GPP in the southeast was higher than the overall mean (1092 gC m^{-2} yr^{-1}), and GPP in the northwest was overall lower than 200 gC m^{-2} yr^{-1} (Table S5 and Fig. 2). The GPP of 57.9 % of the grid cells (1,935,386 grid cells) had a significant upward trend (Fig. S4). The GPP of >50 % of the grid cells in 70 % of the MCs showed a significant upward trend, indicating the carbon sequestration of urban vegetation was significantly enhanced.

The GPP in UAs was generally lower than in RAs, but the GPP growth rate was higher in UAs (Fig. 3a and Fig. S5). GPP increased from 316 gC m^{-2} yr^{-1} in 2000 to 662 gC m^{-2} yr^{-1} in 2018 in UAs, with an annual increase of 20 gC m^{-2} yr^{-2}. GPP increased from 965 gC m^{-2} yr^{-1} in 2000 to 1214 gC m^{-2} yr^{-1} in 2018 in RAs, with an annual increase of 12.75 gC m^{-2} yr^{-2}. We normalized the mean GPP over the years, and found that GPP in the UAs and RAs both had a fluctuating upward trend from 2000 to 2018, while the fluctuation in GPP in the RAs was larger than in the UAs at the same stage (Fig. 3b). Also, GPP had a downward trend in RAs in Xining and Nanjing ($P > 0.05$) (Table S6).

We compared the stability of GPP in UAs and RAs using the adjacent-varying fluctuations F_σ and F_s. Overall, the F_σ in UAs and RAs were 0.05 and 0.12, and F_s were 1.13 and 2.02, respectively (Fig. 3c). Both F_σ and F_s in UAs were smaller than those in RAs, which indicated that the fluctuation of GPP in UA was small and the change was relatively stable. Except for Yinchuan and Lhasa, the fluctuation in UAs was smaller than in RAs in other MCs, which indicated that the GPP in UAs was on a steady upward trend and that UAs had relatively stable environments for urban vegetation due to the positive impact of urbanization (Table S6 and Fig. S6).

3.2. Contributions of climate change and human activities to GPP in UA and RA

A complex non-linear relationship exists between GPP and climatic factors (Fig. 4). Fig. 4(a) and (e) reveal that GPP increases with rising *T*. However, beyond a certain threshold, the rate of change in GPP diminishes, indicating a saturation point where the carbon sequestration capacity of vegetation gradually stabilizes. Analyzing the relationship between GPP and *PR* (Fig. 4(b) and (f)), an increase in GPP is observed as *PR* in UA exceeds 400 mm, but a shift from positive to negative correlation occurs. Similarly, in RA, GPP increases with increasing *PR* when it is below 200 mm, but subsequently exhibits no significant change. These findings suggest that in urban areas, vegetation's carbon sequestration capacity is susceptible to precipitation levels, whereas, in RA, the impact of rainfall on vegetation's carbon sequestration capacity is relatively minimal. Fig. 4(c) and (g) illustrated that with ET_0 values below 50 mm, the vegetation showed a relatively weaker ability for carbon sequestration, whereas a stronger capacity was observed when ET_0 reaches 160 mm. Fig. 4(d) and (h) also vividly depict the contrasting relationship between GPP and *AET* in UA and RA. There exists a distinct linear relationship between the carbon sequestration capacity of vegetation and *AET* in UA. In contrast, the carbon sequestration of vegetation may be constrained once *AET* reaches a certain threshold in RA. These findings further emphasize the substantial role of urban vegetation in carbon sequestration and its crucial contribution to the carbon cycle.

A total of 70 multiple regression models were constructed in this

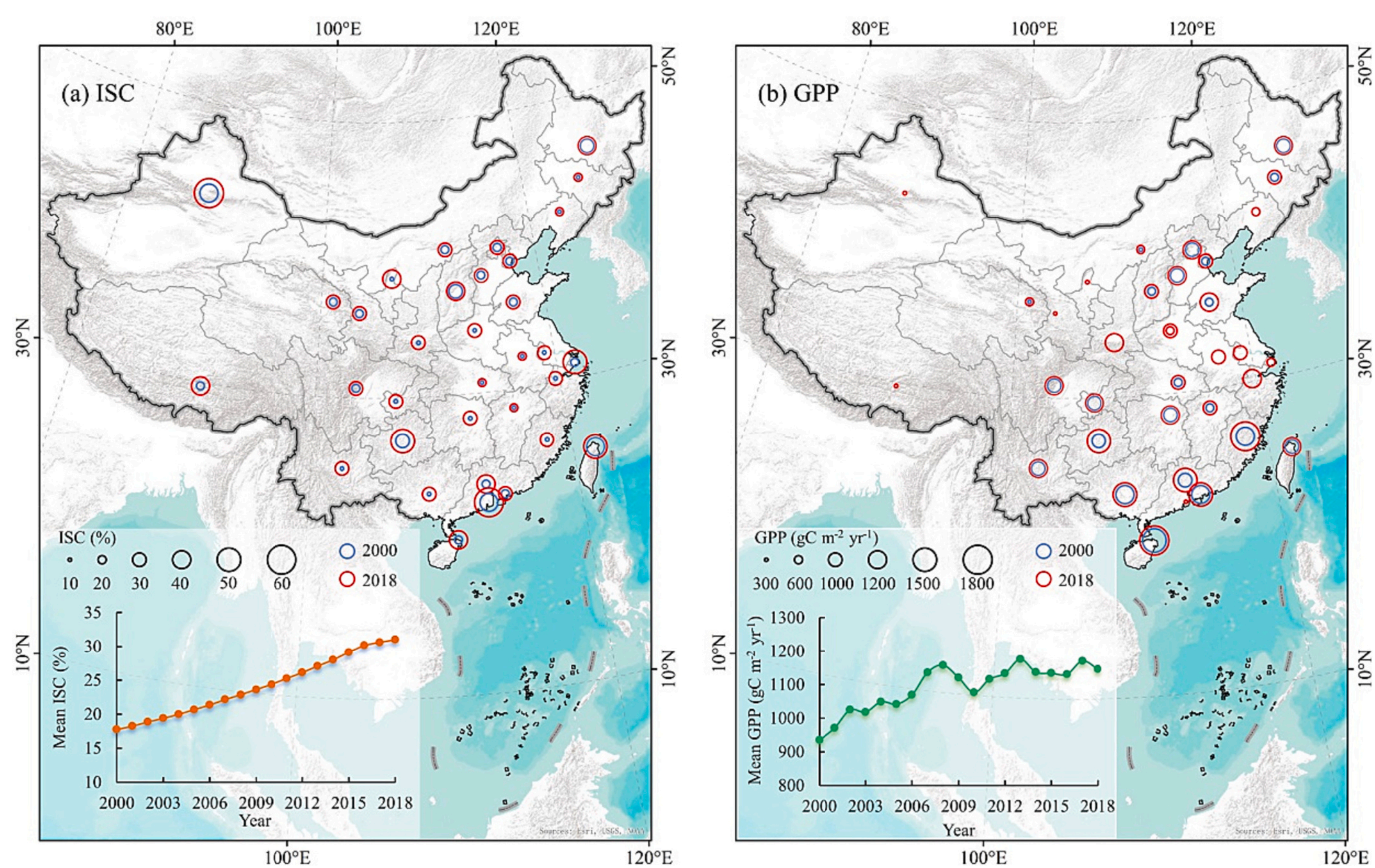

Fig. 2. Changes of ISC (a) and GPP (b) in the 34 MCs from 2000 to 2018.

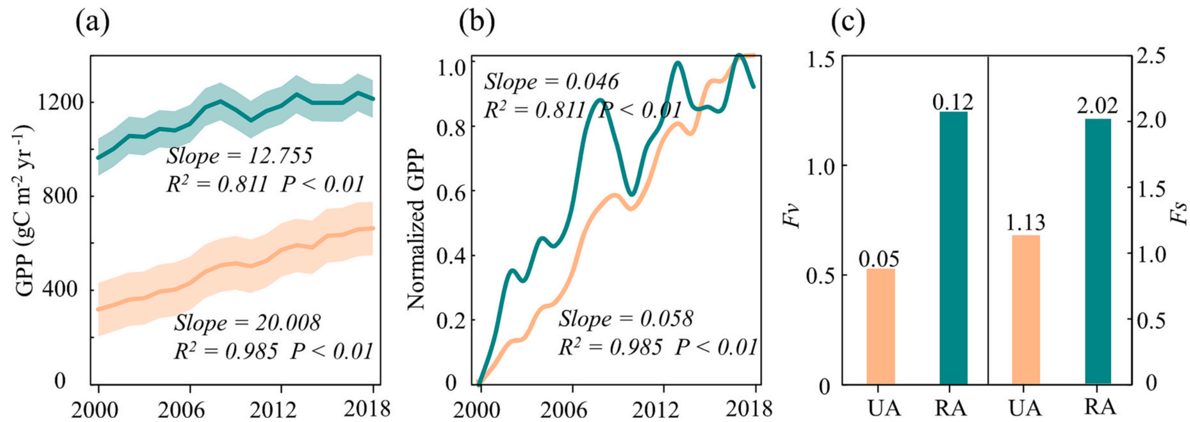

Fig. 3. Changes of annual GPP (a) and normalized GPP (b), and adjacent-varying fluctuations *Fv* and *Fs* (c) in UA and RA from 2000 to 2018.

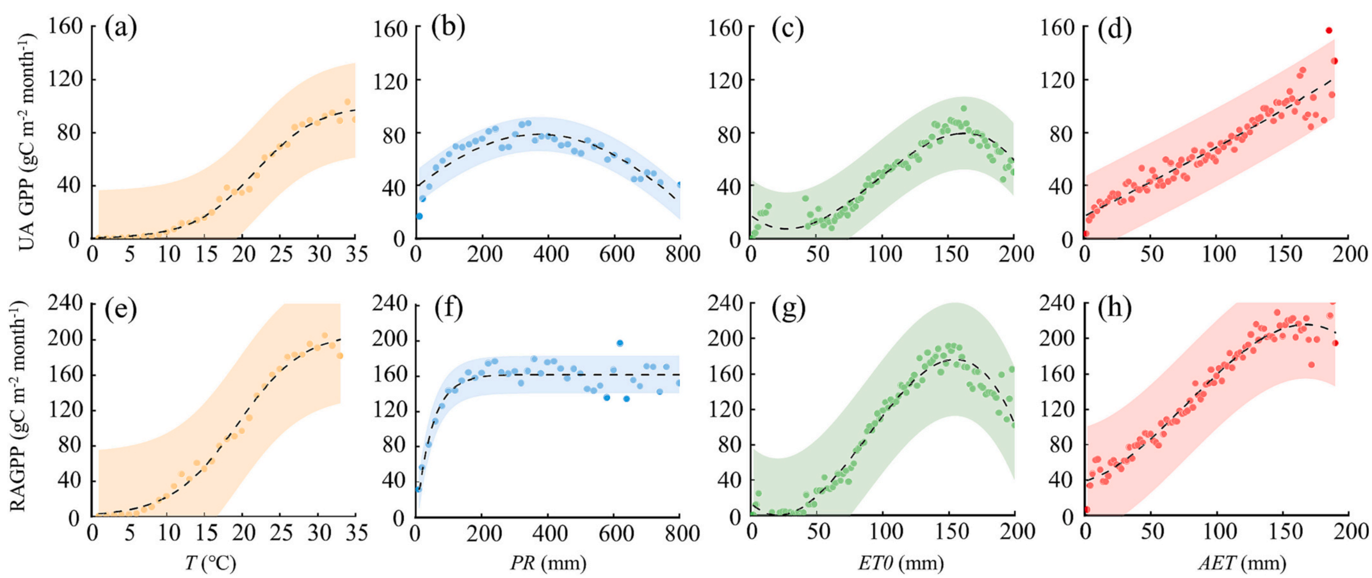

Fig. 4. The relationship between GPP and T, PR, ET_0, and AET. The scatter points were obtained by binning the monthly mean GPP values of MC from 2000 to 2018 based on the x-axis, and then optimal fitting was performed on these scatter points. Black dashed line indicates the mean trend.

study, explaining 79 % of the variation in mean GPP (Tables S7 and S8). Then, according to the multiple regression models, the effects of climate change and human activities on GPP were quantified (Table S9). The results showed that climate change and human activities jointly affected GPP, but there were large differences in their contributions to changes in GPP due to differences in the development stages of the 34 MCs. Overall, GPP was mainly promoted by climate change and human activities, both of which were moderately promoted in UAs, while the GPP in RAs was mainly promoted by climate change. GPP in UAs was mainly promoted by human activities in economically developed cities such as Beijing, Shanghai, Tianjin, and Chongqing, and GPP in RAs was mainly promoted by climate change in the northern cities of China, while there was a negative impact in cities such as Harbin, Xining, and Urumqi.

The contribution of human activities to GPP was comparable to or even greater than that of climate change in UAs, while changes in RAs were dominated by climate change. The contribution of climate change and human activities to GPP was 49 % and 51 % in UAs, respectively, and 76 % and 24 % in RAs (Fig. 5). Of the 34 MCs, 94 % were more greatly impacted by the contribution of human activities to GPP than climate change, while the contributions of human activities and climate change were quite different in RAs. GPP in RAs had a downward trend in Nanjing, which was due to the combined inhibition of vegetation growth by climate change and human activities, but the inhibition impact was not obvious (Table S9).

3.3. The impact and compensation of urbanization on GPP

Our analysis of the relationship between ISC and GPP (ISC ~ GPP) in 2000 and 2018 showed that 70 % and 75 % of the mean GPP values were above the zero-impact line, respectively, and urbanization had a positive impact on GPP (Fig. S7). However, the ISC ~ GPP of the 34 MCs was quite different, and the distribution of GPP along the ISC was relatively scattered because of the small number of corresponding grid cells in a few cities (Fig. 6 and Table S10). Except for Macau and Lhasa, the three regressions of the ISC ~ GPP for all MCs were statistically significant ($P < 0.05$).

In addition to the direct impact on GPP, urbanization also indirectly impacted GPP. Overall, the indirect impact of urbanization on GPP (ω_i) was positive overall and increased superlinearly (Fig. 7a). The mean indirect impacts of urbanization on GPP in 2000 and 2018 were 11.3 % and 15.45 %, respectively, of which ISC was the node where ω_i changed at 20 %. When ISC < 20 %, ω_i was generally small and in a stable state, and when ISC > 20 %, with the increase of ISC, ω_i gradually increased. After reaching the peak, ω_i decreased rapidly, which indicated that with increased ISC, the indirect impact of urbanization on vegetation gradually increased. But after a certain level, the indirect impact decreased

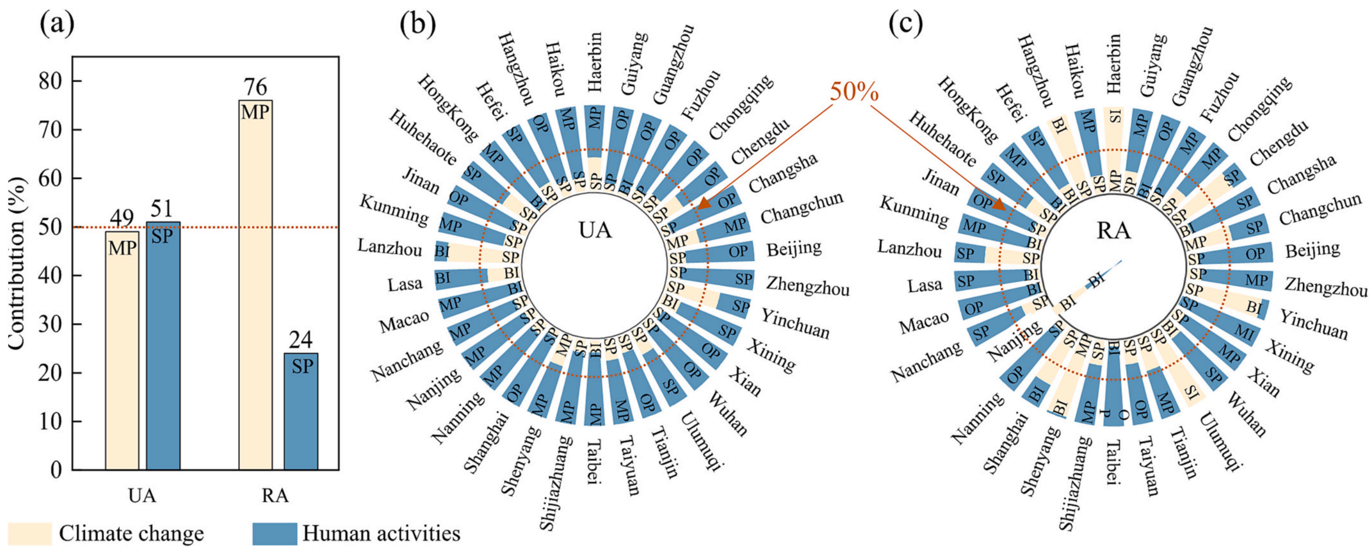

Fig. 5. The contribution of climate change and human activities to GPP. (a) Different contributions of climate change and human activities to GPP in UAs and RAs, respectively; (b) is the contributions of climate change and human activities to the GPP in the 34 MCs in UA, and (c) is that in RA. OI: Obvious inhibition; MI: Moderate inhibition; SI: Slight inhibition; BI: Basically no impact; SP: Slight promotion; MP: Moderate promotion; and OP: Obvious promotion. The dotted orange line in (a) and the dotted circles in (b) and (c) represent a contribution of 50 %.

rapidly. Most MCs had an indirect impact on GPP in China, which promoted vegetation growth, and this indirect impact was more obvious in 2018 (Fig. S8 and Table S11).

The growth offset τ in 2000 and 2018 indicated that the indirect impact of urbanization offset the direct impact as ISC grew, after which τ weakened (Fig. 7b). Overall, τ increased from 4.96 % in 2000 to 12.35 % in 2018, which indicated that the indirect impact of urbanization gradually became more evident (Table S12). During the expansion of most cities in China, vegetation growth improved due to the indirect impact of urbanization despite the increase in impervious surfaces (Fig. S9).

4. Discussion

4.1. Differences in GPP changes between UA and RA

In recent years, numerous studies have shown that both climate change and human activities play significant roles in vegetation growth (Liu et al., 2018a; Ge et al., 2021; Gao et al., 2022; Shi et al., 2021; Tang et al., 2020; Zheng et al., 2019). In this study, overall, human activities had a slightly higher impact on GPP than climate change in UAs, and in RAs the impact of climate change on GPP was much higher than the impact of human activities. However, the extent of their impact varies depending on the geographical location (Fig. 5). For instance, in the southwestern region of China, including Guiyang, Kunming, and Nanning, the influence of human activities differs significantly from that of climate change. The impact level of climate change is classified as SP and BI, while the promotion level of human activities is categorized as MP and OP. Research has demonstrated that the implementation of large-scale ecological restoration projects, such as afforestation and reforestation, has proven effective in the ecological recovery of the southwestern region of China (Wang et al., 2015). On the other hand, in the northeastern region of China, including Shenyang, Harbin, and Changchun, the influence of climate change on vegetation carbon sequestration is noteworthy. The impact level of climate change is classified as MP, while the impact levels of human activities range from BI to SI and SP. Among them, precipitation emerges as the primary controlling factor for vegetation growth (Xue et al., 2022).

GPP had different characteristics in UAs and RAs due to the combined impact of climate change and human activities (Ge et al., 2021; Naeem et al., 2020; Hua et al., 2017). UAs represent the expansion of urban land, the continuous increase of population, and the complexity of urban green space landscapes, while RAs are dominated by natural and semi-natural ecological landscapes (Tang et al., 2020). The higher and more stable fluctuation of GPP indicated that the positive impact of UMC can offset part of the impact of natural environment fluctuations on vegetation in UAs, making it a suitable environment for vegetation growth (Fig. 3 and Fig. S4) (Jiang et al., 2017b). We found that the fluctuation of GPP in UAs was significantly smaller than that in RAs, which indicated that UAs provided a relatively stable environment for vegetation growth, and the urban environment is suitable for GPP (Ruan et al., 2019). Moreover, a recent study based on urban grid cells and GPP VPM analysis showed that the interannual fluctuation of global urban GPP was also smaller than that of non-urban GPP, and indicated that our study was consistent at larger spatial scales (Cui et al., 2022). Furthermore, China exhibits significant variations in climate background, urbanization levels, and urban environments (Yang et al., 2020; Chen et al., 2022). In this study, we also quantified the fluctuation of GPP in UAs and RAs more precisely and highlighted the differences in the impact of urban and rural environments on vegetation growth (Fig. 3 and Fig. S5). Among them, Shanghai, Hangzhou, and Nanjing show significant differences in urban-rural vegetation fluctuations, primarily due to higher GPP values of *Fv* and *Fs* in these regions, which are mainly driven by rapid urbanization. In addition, the intricacies of our study area's geographical location and topographical attributes have contributed to a rich tapestry of climatic patterns. In turn, this gives rise to sporadic occurrences of extreme weather events, exemplified by instances of heavy precipitation episodes (Wang et al., 2019).

4.2. The impact of urbanization on vegetation

We found that GPP had a significant upward trend in China's quickly developing UAs. Moreover, the impact of urbanization on GPP became more positive over time, and was related to landscape patterns and urban local microclimate. Many scholars focused on the reduction of vegetation area caused by urbanization due to land use conversion (Deng and Zhu, 2020; De Carvalho and Szlafsztein, 2019; Liu et al., 2018b; Tian and Qiao, 2014). In recent years, more and more scholars, both globally and regionally, have reported that there are not only negative impacts of reducing vegetation coverage in urbanization but

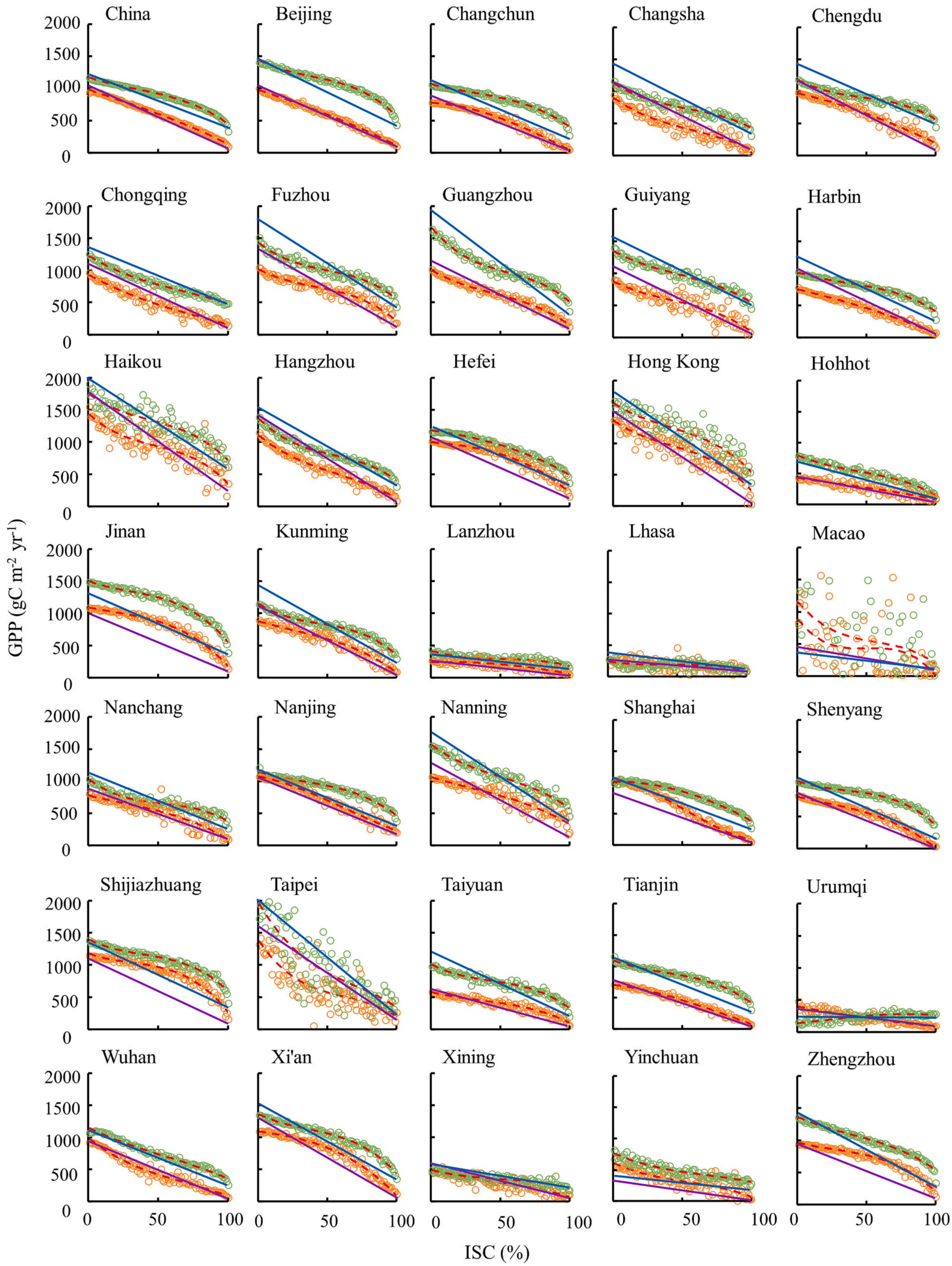

Fig. 6. Changes in GPP with ISC in 2000 and 2018. The points in the graph represent the average values of GPP within a 1 % ISC interval. The red dotted line represents the fitted curve, the orange circle represents the mean GPP in 2000, the green circle represents the mean GPP in 2018, the purple line represents the zero-impact line in 2000, and the blue line represents the zero-impact line in 2018.

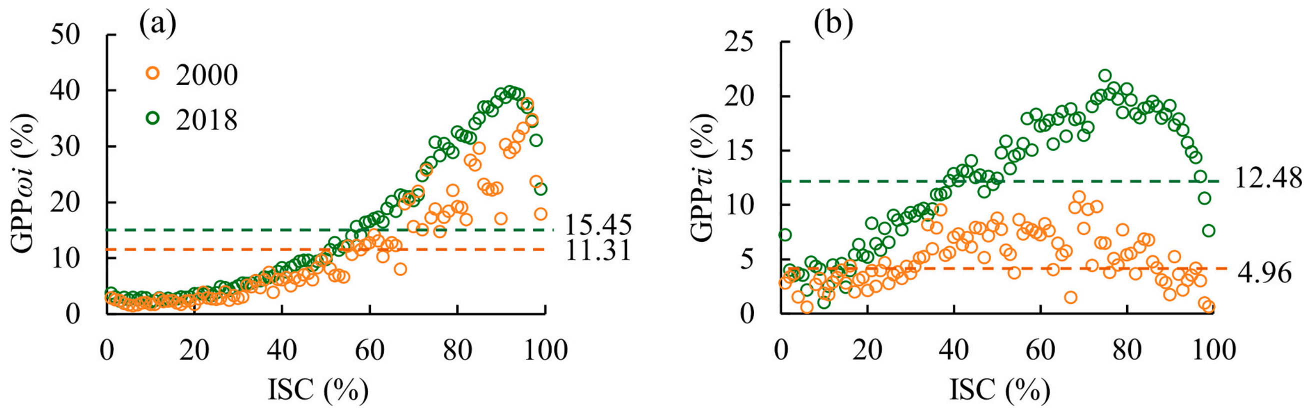

Fig. 7. Change in indirect impact percentage (a) and growth offset (b) difference between 2000 and 2018.

also positive impacts such as increased urban vegetation greenness and carbon sequestration (Sun et al., 2020; Chen et al., 2021a, 2021b; Wei et al., 2021; Zhao et al., 2016; Zhong et al., 2019). Simultaneously, urbanization-caused CO_2 emissions, in turn, give rise to a fertilization effect on vegetation (Chen et al., 2021a, 2021b). Considering that the GPP data used from actual remote sensing observations of vegetation growth and the impact of CO_2 on GPP has already been reflected in GPP to a certain extent, this study does not discuss this separately. Additionally, through irrigation and cultivation of vegetation within urban areas, coupled with substantial light refraction on building surfaces, these combined processes enhance the photosynthetic capacity of urban vegetation, consequently extending the duration of the growing season (Luo et al., 2021; He et al., 2021; Yang et al., 2021; Du et al., 2019; Ding et al., 2021). Thus, it is only by exploring the impact of urbanization on vegetation photosynthesis under climate change and human activities in a wider range to discover the inherent impact of the urban environment on vegetation and explore whether this impact is universal (Zhao et al., 2016). Differences in GDP growth, population changes, and UMC between cities lead to differences in their contributions across cities in different regions (Zhang et al., 2021; Zhang and Ye, 2021; Sun et al., 2020). More developed cities have higher requirements for urban ecological environments and invest a lot of money to build urban green spaces, open spaces, and parks (Zhang et al., 2021). Urban core areas in cities with higher GDP, such as Beijing, Shanghai, Tianjin, Guangzhou, Fuzhou, Chongqing, Xi'an, and Changsha, prioritize environmental improvement. The carbon sequestration function of urban vegetation in these urban agglomerations (UAs) is mainly driven by human activities (Fig. 5) (Zhang et al., 2021; Chaparro et al., 2018; Li et al., 2018; Li et al., 2020). It is worth noting that GPP has declined in the Yangtze River Delta, including Hangzhou and Nanjing, indicating regional variations in urbanization and the ecological environment (Du et al., 2019; Shao et al., 2020). This can be attributed to rapid urbanization along the Yangtze River (Fig. S3) (Qu et al., 2020). Thus, on the one hand, the continuous increase in GPP can be maintained in UAs, on the other hand, the positive impact of urbanization on GPP is continuously enhanced, which relies upon good urban landscape planning and vegetation management and protection.

4.3. Quantifying fluctuations and factors influencing vegetation growth

Several studies have demonstrated that precipitation and temperature play significant roles as the primary drivers of GPP in Asian ecosystems (Kato and Tang, 2008; Jiang et al., 2017a; Ge et al., 2021; Huang et al., 2020). Compared to previous studies that primarily focused on analyzing the impact of climate factors on vegetation growth using only two to three variables such as temperature or precipitation (Zheng et al., 2021; Chen et al., 2021a, 2021b; Huang et al., 2020), our study integrates key factors from previous relevant studies and considers a total of four factors: temperature, precipitation, reference evapotranspiration, and actual evapotranspiration. Then, we used partial correlation coefficients to filter out unique climatic factors in 34 MCs to simulate the response of vegetation to climate change. Nevertheless, considering only four factors is not comprehensive enough to still be a flaw of our study. In fact, the carbon sequestration capacity of vegetation is also dependent on solar radiation (Zhang et al., 2021; Ge et al., 2021) and sunshine duration (Wang et al., 2015), further refinement and analysis for the impacts of climate change and human activities are thus needed to comprehensively assess their respective impacts on urban vegetation carbon sequestration. Additionally, due to the influence of urban heat island effects and urban footprints, the scope of the urban climate boundary extends far beyond the physical boundaries of the city, necessitating the effective differentiation of the effects between the physical and climate boundaries of the city in the future. Residual trend analysis is a widely used quantitative method for analyzing these factors (Zheng et al., 2019; Ge et al., 2021; Jiang et al., 2017a, 2017b). However, despite its convenience, this method only considers climate change and human activities, neglecting other factors that can influence vegetation growth and carbon sequestration potential. Given that cities are complex systems, a more refined modeling approach is required (Liu et al., 2019).

The fluctuation of GPP can reflect whether the regional environment provides a more suitable environment for vegetation growth. In previous studies, the standard deviation was generally used to compare the degree of dispersion of two or more groups of data. At the same time, when the measurement scales of the data were significantly different or the dimensions were different, the coefficient of variation was used, but the two did not reflect the degree of fluctuation of the data over time, especially for the fluctuation of adjacent years (Zhang et al., 2007; Bedeian and Mossholder, 2000). Thus, we innovatively proposed adjacent-varying fluctuations to quantify the fluctuation of GPP in UAs and RAs, which not only considered the continuity of the data over time, but also eliminated the dimension problem caused by the difference of the original value (e.g., the fluctuation value 50 with original value 60 is much larger than the fluctuation value 50 with original value 600, and this method of adjacent-varying fluctuation can eliminate the fluctuation difference through normalization).

5. Conclusion

We divided China's 34 MCs into UAs and RAs, analyzed the differences in GPP impacted by climate change and human activities from 2000 to 2018, and quantified the impact of urbanization on vegetation. We found that with the growth of ISC, GPP had an upward trend as a whole in UAs and RAs from 2000 to 2018, with an annual increase of 20 gC m^{-2} yr^{-2} and 12.75 gC m^{-2} yr^{-2}. The GPP in UAs had a steady upward trend, which was mainly impacted positively by climate change and human activities, and the contribution of human activities to vegetation is slightly higher than that of climate change. The contribution of climate change and human activities to GPP in 2000 and 2018 were 49 % and 51 %, respectively, and in RAs these contributions to GPP were 76 % and 24 %, respectively. The direct impact of land use conversion caused by urbanization on GPP was offset by indirect impacts, which were 4.96 % and 12.35 % in 2000 and 2018, respectively. The difference between these offsets and changes in GPP in cities was mainly due to the degree of urbanization and differences in urban climate and management.

Our research findings demonstrate that human activities within urban areas play a significant role in vegetation carbon sinks. Therefore, enhancing urban greening and creating a more favorable environment for vegetation growth should be prioritized in urbanization efforts to continually enhance the carbon sequestration capacity of urban ecosystems. The framework of this study possesses universality and applicability, allowing for its generalization to a broader range of contexts, which aids in a more accurate assessment of urban vegetation carbon sequestration potential. Considering the multitude of factors involved in climate change and human activities, including both direct and indirect impacts, future research should deepen our understanding of vegetation carbon sequestration and conduct more detailed analytical studies to comprehensively comprehend and evaluate the contributions of climate change and human activities to urban carbon cycling.

CRediT authorship contribution statement

Xiaoyan Liu: Conception and design, acquisition of data, analysis and interpretation of data, and drafting the manuscript.

Yaoping Cui: Conception and design, and revising the manuscript for important intellectual content.

Wanlong Li: Acquisition of data.

Mengdi Li: Revising the manuscript.

Nan Li: Acquisition of data.

Zhifang Shi: Acquisition of data.

Jinwei Dong: Revising the manuscript for important intellectual content.

Xiangming Xiao: Conception and design, and revising the manuscript for important intellectual content.

Declaration of competing interest

The authors declare that they have no known competing financial interests or personal relationships that could have appeared to influence the work reported in this paper.

Data availability

Global gross primary (GPP) data are publicly available by https://doi.pangaea.de/10.1594/PANGAEA.928381. Impervious surface (IS) data can be downloaded from http://data.ess.tsinghua.edu.cn.

Acknowledgments

This work was supported in part by the National Natural Science Foundation of China (42071415), Xinyang Institute of Ecology 2023 Open Fund (2023XYMS014), Central Plains Talent Program (Cultivate talents): Top-notch young talents of Central Plains and Excellent Textbook Project for Graduate Students in Henan Province (YJS2023JC22), U.S. National Science Foundation (1911955), and Postgraduate Cultivating Innovation and Quality Improvement Action Plan of Henan University (SYLYC2022011).

Appendix A. Supplementary data

Supplementary data to this article can be found online at https://doi.org/10.1016/j.scitotenv.2023.166490.

References

Abatzoglou, J.T., Dobrowski, S.Z., Parks, S.A., Hegewisch, K.C., 2018. TerraClimate, a high-resolution global dataset of monthly climate and climatic water balance from 1958–2015. Sci Data 5 (1), 1–12. https://doi.org/10.1038/sdata.2017.191.

Ahlström, A., Schurgers, G., Arneth, A., Smith, B., 2012. Robustness and uncertainty in terrestrial ecosystem carbon response to CMIP5 climate change projections. Environ. Res. Lett. 7 (4), 044008 https://doi.org/10.1088/1748-9326/7/4/044008.

Anav, A., Friedlingstein, P., Beer, C., Ciais, P., Harper, A., Jones, C., et al., 2015. Spatiotemporal patterns of terrestrial gross primary production: a review. Rev. Geophys. 53 (3), 785–818. https://doi.org/10.1002/2015RG000483.

Bedeian, A.G., Mossholder, K.W., 2000. On the use of the coefficient of variation as a measure of diversity. Organ. Res. Methods 3 (3), 285–297. https://doi.org/10.1177/109442810033005.

Berner, L.T., Goetz, S.J., 2022. Satellite observations document trends consistent with a boreal forest biome shift. Glob. Chang. Biol. 28 (10), 275–3292. https://doi.org/10.1111/gcb.16121.

Chaparro, D., Piles, M., Vall-Llossera, M., Camps, A., Konings, A.G., Entekhabi, D., 2018. L-band vegetation optical depth seasonal metrics for crop yield assessment. Remote Sens. Environ. 212, 249–259. https://doi.org/10.1016/j.rse.2018.04.049.

Chen, J., Jönsson, P., Tamura, M., Gu, Z., Matsushita, B., Eklundh, L., 2004. A simple method for reconstructing a high-quality NDVI time-series data set based on the Savitzky–Golay filter. Remote Sens. Environ. 91 (3–4), 332–344. doi:https://doi.org/10.1016/j.rse.2004.03.014.

Chen, Y., Feng, X., Tian, H., Wu, X., Gao, Z., Feng, Y., et al., 2021a. Accelerated increase in vegetation carbon sequestration in China after 2010: a turning point resulting from climate and human interaction. Glob. Chang. Biol. 27 (22), 5848–5864. https://doi.org/10.1111/gcb.15854.

Chen, S., Zhang, Y., Wu, Q., Liu, S., Song, C., Xiao, J., et al., 2021b. Vegetation structural change and CO_2 fertilization more than offset gross primary production decline caused by reduced solar radiation in China. Agric. For. Meteorol. 296, 108207.

Chen, Y., Huang, B., Zeng, H., 2022. How does urbanization affect vegetation productivity in the coastal cities of eastern China? Sci. Total Environ. 811, 152356 https://doi.org/10.1016/j.scitotenv.2021.152356.

Cui, Y., Xiao, X., Zhang, Y., Dong, J., Qin, Y., Doughty, R.B., et al., 2017. Temporal consistency between gross primary production and solar-induced chlorophyll fluorescence in the ten most populous megacity areas over years. Sci. Rep. 7 (1), 1–12. https://doi.org/10.1038/s41598-017-13783-5.

Cui, Y., Xiao, X., Dong, J., Zhang, Y., Qin, Y., Doughty, R.B., et al., 2022. Continued increases of gross primary production in urban areas during 2000–2016. J. Remote Sens. 2022, 9868564. https://doi.org/10.34133/2022/9868564.

De Carvalho, R.M., Szlafsztein, C.F., 2019. Urban vegetation loss and ecosystem services: the influence on climate regulation and noise and air pollution. Environ. Pollut. 245, 844–852. https://doi.org/10.1016/j.envpol.2018.10.114.

Deng, C., Zhu, Z., 2020. Continuous subpixel monitoring of urban impervious surface using Landsat time series. Remote Sens. Environ. 238, 110929 https://doi.org/10.1016/j.rse.2018.10.011.

Ding, Z., Zheng, H., Li, H., Yu, P., Man, W., Liu, M., et al., 2021. Afforestation-driven increases in terrestrial gross primary productivity are partly offset by urban expansion in Southwest China. Ecol. Indic. 127, 107641 https://doi.org/10.1016/j.ecolind.2021.107641.

Doughty, R., Xiao, X., Köhler, P., Frankenberg, C., Qin, Y., Wu, X., et al., 2021. Global-scale consistency of spaceborne vegetation indices, chlorophyll fluorescence, and photosynthesis. J. Geophys. Res. Biogeosci. 126 (6) https://doi.org/10.1029/2020JG006136 e2020JG006136.

Du, J., Fu, Q., Fang, S., Wu, J., He, P., Quan, Z., 2019. Effects of rapid urbanization on vegetation cover in the metropolises of China over the last four decades. Ecol. Indic. 107, 105458 https://doi.org/10.1016/j.ecolind.2019.105458.

Evans, J., Geerken, R., 2004. Discrimination between climate and human-induced dryland degradation. J. Arid Environ. 57 (4), 535–554. https://doi.org/10.1016/S0140-1963(03)00121-6.

Fontana, F., Rixen, C., Jonas, T., Aberegg, G., Wunderle, S., 2008. Alpine grassland phenology as seen in AVHRR, VEGETATION, and MODIS NDVI time series-a comparison with in situ measurements. Sensors 8 (4), 2833–2853. https://doi.org/10.3390/s8042833.

Gao, W., Zheng, C., Liu, X., Lu, Y., Chen, Y., Wei, Y., et al., 2022. NDVI-based vegetation dynamics and their responses to climate change and human activities from 1982 to 2020: a case study in the mu us sandy land, China. Ecol. Indic. 137, 108745 https://doi.org/10.1016/j.ecolind.2022.108745.

Garbulsky, M.F., Peñuelas, J., Papale, D., Ardö, J., Goulden, M.L., Kiely, G., et al., 2010. Patterns and controls of the variability of radiation use efficiency and primary productivity across terrestrial ecosystems. Glob. Ecol. Biogeogr. 19 (2), 253–267. https://doi.org/10.1111/j.1466-8238.2009.00504.x.

Ge, W., Deng, L., Wang, F., Han, J., 2021. Quantifying the contributions of human activities and climate change to vegetation net primary productivity dynamics in China from 2001 to 2016. Sci. Total Environ. 773, 145648 https://doi.org/10.1016/j.scitotenv.2021.145648.

Gong, P., Li, X., Wang, J., Bai, Y., Chen, B., Hu, T., et al., 2020. Annual maps of global artificial impervious area (GAIA) between 1985 and 2018. Remote Sens. Environ. 236, 111510 https://doi.org/10.1016/j.rse.2019.111510.

Grimm, N.B., Faeth, S.H., Golubiewski, N.E., Redman, C.L., Wu, J., Bai, X., et al., 2008. Global change and the ecology of cities. Science 319 (5864), 756–760. https://doi.org/10.1126/science.1150195.

Gu, Z., Duan, X., Shi, Y., Li, Y., Pan, X., 2018. Spatiotemporal variation in vegetation coverage and its response to climatic factors in the Red River Basin, China. Ecol. Indic. 93, 54–64.

Hammond, W.M., Williams, A.P., Abatzoglou, J.T., Adams, H.D., Klein, T., López, R., et al., 2022. Global field observations of tree die-off reveal hotter-drought fingerprint for Earth's forests. Nat. Commun. 13 (1), 1761. https://doi.org/10.1038/s41467-022-29289-2.

He, X., Yu, Y., Cui, Z., He, T., 2021. Climate change and ecological projects jointly promote vegetation restoration in three-river source region of China. Chin. Geogr. Sci. 31, 1108–1122. https://doi.org/10.1007/s11769-021-1245-1.

Hua, W., Chen, H., Zhou, L., Xie, Z., Qin, M., Li, X., et al., 2017. Observational quantification of climatic and human influences on vegetation greening in China. Remote Sens. 9 (5), 425. https://doi.org/10.3390/rs9050425.

Huang, S., Zheng, X., Ma, L., Wang, H., Huang, Q., Leng, G., et al., 2020. Quantitative contribution of climate change and human activities to vegetation cover variations based on GA-SVM model. J. Hydrol. 584, 124687 https://doi.org/10.1016/j.jhydrol.2020.124687.

Jiang, L., Bao, A., Guo, H., Ndayisaba, F., 2017a. Vegetation dynamics and responses to climate change and human activities in Central Asia. Sci. Total Environ. 599, 967–980. https://doi.org/10.1016/j.scitotenv.2017.05.012.

Jiang, M., Tian, S., Zheng, Z., Zhan, Q., He, Y., 2017b. Human activity influences on vegetation cover changes in Beijing, China, from 2000 to 2015. Remote Sens. 9 (3), 271. https://doi.org/10.3390/rs9030271.

Karger, D.N., Conrad, O., Böhner, J., Kawohl, T., Kreft, H., Soria-Auza, R.W., et al., 2017. Climatologies at high resolution for the earth's land surface areas. Sci Data 4 (1), 1–20. https://doi.org/10.1038/sdata.2017.122.

Kato, T., Tang, Y., 2008. Spatial variability and major controlling factors of CO2 sink strength in Asian terrestrial ecosystems: evidence from eddy covariance data. Glob. Chang. Biol. 14 (10), 2333–2348. https://doi.org/10.1111/j.1365-2486.2008.01646.x.

Khon, V.C., Mokhov, I.I., Roeckner, E., Semenov, V.A., 2007. Regional changes of precipitation characteristics in northern Eurasia from simulations with global climate model. Glob. Planet 57 (1–2), 118–123. https://doi.org/10.1016/j.gloplacha.2006.11.006.

Li, F., Wang, X., Liu, H., Li, X., Zhang, X., Sun, Y., et al., 2018. Does economic development improve urban greening? Evidence from 289 cities in China using spatial regression models. Environ. Monit. Assess. 190, 1–19. https://doi.org/10.1007/s10661-018-6871-4.

Li, D., Wu, S., Liang, Z., Li, S., 2020. The impacts of urbanization and climate change on urban vegetation dynamics in China. Urban For. Urban Green. 54, 126764 https://doi.org/10.1016/j.ufug.2020.126764.

Li, H., Yang, B., Meng, Y., Liu, K., Wang, S., Wang, D., et al., 2023. Relationship between carbon pool changes and environmental changes in arid and semi-arid steppe—a two decades study in Inner Mongolia, China. Sci. Total Environ. 893, 164930 https://doi.org/10.1016/j.scitotenv.2023.164930.

Liu, R., Xiao, L., Liu, Z., Dai, J., 2018a. Quantifying the relative impacts of climate and human activities on vegetation changes at the regional scale. Ecol. Indic. 93, 91–99. https://doi.org/10.1016/j.ecolind.2018.04.047.

Liu, S., Du, W., Su, H., Wang, S., Guan, Q., 2018b. Quantifying impacts of land-use/cover change on urban vegetation gross primary production: a case study of Wuhan, China. Sustainability 10 (3), 714. https://doi.org/10.3390/su10030714.

Liu, Y., Zhou, G., Du, H., Berninger, F., Mao, F., Li, X., et al., 2018c. Response of carbon uptake to abiotic and biotic drivers in an intensively managed lei bamboo forest. J. Environ. Manag. 223, 713–722. https://doi.org/10.1016/j.jenvman.2018.06.046.

Liu, X., Pei, F., Wen, Y., Li, X., Wang, S., Wu, C., et al., 2019. Global urban expansion offsets climate-driven increases in terrestrial net primary productivity. Nat. Commun. 10 (1), 1–8. https://doi.org/10.1038/s41467-019-13462-1.

Liu, Y., Liu, H., Chen, Y., Gang, C., Shen, Y., 2022. Quantifying the contributions of climate change and human activities to vegetation dynamic in China based on multiple indices. Sci. Total Environ. 156553 https://doi.org/10.1016/j.scitotenv.2022.156553.

Luo, Y., Sun, W., Yang, K., Zhao, L., 2021. China urbanization process induced vegetation degradation and improvement in recent 20 years. Cities 114, 103207. https://doi.org/10.1016/j.cities.2021.103207.

Lutz, J.A., Van Wagtendonk, J.W., Franklin, J.F., 2010. Climatic water deficit, tree species ranges, and climate change in Yosemite National Park. J. Biogeogr. 37 (5), 936–950. https://doi.org/10.1111/j.1365-2699.2009.02268.x.

Ma, J., Xiao, X., Zhang, Y., Doughty, R., Chen, B., Zhao, B., 2018. Spatial-temporal consistency between gross primary productivity and solar-induced chlorophyll fluorescence of vegetation in China during 2007–2014. Sci. Total Environ. 639, 1241–1253. https://doi.org/10.1016/j.scitotenv.2018.05.245.

Miller, D.L., Roberts, D.A., Clarke, K.C., Lin, Y., Menzer, O., Peters, E.B., et al., 2018. Gross primary productivity of a large metropolitan region in midsummer using high spatial resolution satellite imagery. Urban Ecosyst. 21, 831–850. https://doi.org/10.1007/s11252-018-0769-3.

Naeem, S., Zhang, Y., Tian, J., Qamer, F.M., Latif, A., Paul, P.K., 2020. Quantifying the impacts of anthropogenic activities and climate variations on vegetation productivity changes in China from 1985 to 2015. Remote Sens. 12 (7), 1113. https://doi.org/10.3390/rs12071113.

Nuarsa, I.W., As-syakur, A.R., Gunadi, I.G.A., Sukewijaya, I.M., 2018. Changes in gross primary production (GPP) over the past two decades due to land use conversion in a Tourism City. ISPRS Int. J. Geo-Inf. 7 (2), 57. https://doi.org/10.3390/ijgi7020057.

Ou, J., Liu, X., Li, X., Chen, Y., 2013. Quantifying the relationship between urban forms and carbon emissions using panel data analysis. Landsc. Ecol. 28, 1889–1907. https://doi.org/10.1007/s10980-013-9943-4.

Qu, S., Wang, L., Lin, A., Yu, D., Yuan, M., 2020. Distinguishing the impacts of climate change and anthropogenic factors on vegetation dynamics in the Yangtze River Basin, China. Ecol. Indic. 108, 105724 https://doi.org/10.1016/j.ecolind.2019.105724.

Ritchie, H., Roser, M., 2018. Urbanization. https://ourworldindata.org/urbanization (accessed 5 March 2022).

Ruan, Y., Zhang, X., Xin, Q., Ao, Z., Sun, Y., 2019. Enhanced vegetation growth in the urban environment across 32 cities in the northern hemisphere. J. Geophys. Res. Biogeosci. 124 (12), 3831–3846. https://doi.org/10.1029/2019JG005262.

Shao, Z., Ding, L., Li, D., Altan, O., Huq, M.E., Li, C., 2020. Exploring the relationship between urbanization and ecological environment using remote sensing images and statistical data: a case study in the Yangtze River Delta, China. Sustainability 12 (14), 5620. https://doi.org/10.3390/su12145620.

Shi, S., Yu, J., Wang, F., Wang, P., Zhang, Y., Jin, K., 2021. Quantitative contributions of climate change and human activities to vegetation changes over multiple time scales on the loess plateau. Sci. Total Environ. 755, 142419 https://doi.org/10.1016/j.scitotenv.2020.142419.

Sun, Y., Yang, Y., Zhang, L., Wang, Z., 2015. The relative roles of climate variations and human activities in vegetation change in North China. Phys. Chem. Earth. Parts A/B/C 87, 67–78. https://doi.org/10.1016/j.pce.2015.09.017.

Sun, L., Chen, J., Li, Q., Huang, D., 2020. Dramatic uneven urbanization of large cities throughout the world in recent decades. Nat. Commun. 11 (1), 1–9. https://doi.org/10.1038/s41467-020-19158-1.

Tan, X., Lai, H., Gu, B., Zeng, Y., Li, H., 2018. Carbon emission and abatement potential outlook in China's building sector through 2050. Energy Policy 118, 429–439. https://doi.org/10.1016/j.enpol.2018.03.072.

Tang, X., Cui, Y., Li, N., Fu, Y., Liu, X., Run, Y., et al., 2020. Human activities enhance radiation forcing through surface albedo associated with vegetation in Beijing. Remote Sens. 12 (5), 837. https://doi.org/10.3390/rs12050837.

Tian, G., Qiao, Z., 2014. Assessing the impact of the urbanization process on net primary productivity in China in 1989–2000. Environ. Pollut. 184, 320–326. https://doi.org/10.1016/j.envpol.2013.09.012.

Velasco, E., Roth, M., Norford, L., Molina, L.T., 2016. Does urban vegetation enhance carbon sequestration? Landsc. Urban Plan. 148, 99–107. https://doi.org/10.1016/j.landurbplan.2015.12.003.

Walker, J.J., De Beurs, K.M., Henebry, G.M., 2015. Land surface phenology along urban to rural gradients in the US Great Plains. Remote Sens. Environ. 165, 42–52. https://doi.org/10.1016/j.rse.2015.04.019.

Wang, J., Wang, K., Zhang, M., Zhang, C., 2015. Impacts of climate change and human activities on vegetation cover in hilly southern China. Ecol. Eng. 81, 451–461. https://doi.org/10.1016/j.ecoleng.2015.04.022.

Wang, X., Min, A., Liao, Y., 2019. Major heavy rainfall events in China from April to October in 2018. Torr. Rain Disasters 38 (2), 183–192. https://doi.org/10.12677/ccrl.2020.96072.

Watts, M., 2017. Cities spearhead climate action. Nat. Clim. Chang. 7 (8), 537–538. https://doi.org/10.1038/nclimate3358.

Wei, S., Chen, Q., Wu, W., Ma, J., 2021. Quantifying the indirect effects of urbanization on urban vegetation carbon uptake in the megacity of Shanghai, China. Environ. Res. Lett. 16 (6), 064088 https://doi.org/10.1088/1748-9326/ac06fd.

Wu, D., Zhao, X., Liang, S., Zhou, T., Huang, K., Tang, B., et al., 2015. Time-lag effects of global vegetation responses to climate change. Glob. Chang. Biol. 21 (9), 3520–3531. https://doi.org/10.1111/gcb.12945.

Xie, S., Mo, X., Hu, S., Liu, S., 2020. Contributions of climate change, elevated atmospheric CO2 and human activities to ET and GPP trends in the three-north region of China. Agric. For. Meteorol. 295, 108183 https://doi.org/10.1016/j.agrformet.2020.108183.

Xue, L., Kappas, M., Wyss, D., Wang, C., Putzenlechner, B., Thi, N.P., et al., 2022. Assessment of climate change and human activities on vegetation development in Northeast China. Sensors 22 (7), 2509. https://doi.org/10.3390/s22072509.

Yang, K., Pan, M., Luo, Y., Chen, K., Zhao, Y., Zhou, X., 2019. A time-series analysis of urbanization-induced impervious surface area extent in the Dianchi Lake watershed from 1988–2017. Int. J. Remote Sens. 40 (2), 573–592. https://doi.org/10.1080/01431161.2018.1516312.

Yang, J., Luo, X., Jin, C., Xiao, X., Xia, J.C., 2020. Spatiotemporal patterns of vegetation phenology along the urban–rural gradient in Coastal Dalian, China. Urban For. Urban Green. 54, 126784 https://doi.org/10.1016/j.ufug.2020.126784.

Yang, Q., Huang, X., Yang, J., Liu, Y., 2021. The relationship between land surface temperature and artificial impervious surface fraction in 682 global cities: spatiotemporal variations and drivers. Environ. Res. Lett. 16 (2), 024032 https://doi.org/10.1088/1748-9326/abdaed.

Zhang, Y., Ye, A., 2021. Quantitatively distinguishing the impact of climate change and human activities on vegetation in mainland China with the improved residual method. GIScience & Remote Sensing 58 (2), 235–260. https://doi.org/10.1080/15481603.2021.1872244.

Zhang, C., Jordan, C., Higgins, A., 2007. Using neighbourhood statistics and GIS to quantify and visualize spatial variation in geochemical variables: an example using Ni concentrations in the topsoils of Northern Ireland. Geoderma 137 (3–4), 466–476. https://doi.org/10.1016/j.geoderma.2006.10.018.

Zhang, Y., Xiao, X., Wu, X., Zhou, S., Zhang, G., Qin, Y., et al., 2017. A global moderate resolution dataset of gross primary production of vegetation for 2000-2016. Sci Data 4 (1), 1–13. https://doi.org/10.1038/sdata.2017.165.

Zhang, W., Randall, M., Jensen, M.B., Brandt, M., Wang, Q., Fensholt, R., 2021. Socio-economic and climatic changes lead to contrasting global urban vegetation trends. Glob. Environ. Chang. 71, 102385 https://doi.org/10.1016/j.gloenvcha.2021.102385.

Zhang, L., Yang, L., Zohner, C.M., Crowther, T.W., Li, M., Shen, F., et al., 2022. Direct and indirect impacts of urbanization on vegetation growth across the world's cities. Sci. Adv. 8 (27), eabo0095. https://doi.org/10.1126/sciadv.abo0095.

Zhao, T., Brown, D.G., Fang, H., Theobald, D.M., Liu, T., Zhang, T., 2012. Vegetation productivity consequences of human settlement growth in the eastern United States. Landsc. Ecol. 27, 1149–1165. https://doi.org/10.1007/s10980-012-9766-8.

Zhao, S., Liu, S., Zhou, D., 2016. Prevalent vegetation growth enhancement in urban environment. Proc. Natl. Acad. Sci. 113 (2), 6313–6318. https://doi.org/10.1073/pnas.1602312113.

Zheng, K., Wei, J.Z., Pei, J.Y., Cheng, H., Zhang, X.L., Huang, F.Q., et al., 2019. Impacts of climate change and human activities on grassland vegetation variation in the Chinese loess plateau. Sci. Total Environ. 660, 236–244. https://doi.org/10.1016/j.scitotenv.2019.01.022.

Zheng, K., Tan, L., Sun, Y., Wu, Y., Duan, Z., Xu, Y., et al., 2021. Impacts of climate change and anthropogenic activities on vegetation change: evidence from typical areas in China. Ecol. Indic. 126, 107648 https://doi.org/10.1016/j.ecolind.2021.107648.

Zhong, Q., Ma, J., Zhao, B., Wang, X., Zong, J., Xiao, X., 2019. Assessing spatial-temporal dynamics of urban expansion, vegetation greenness and photosynthesis in megacity Shanghai, China during 2000–2016. Remote Sens. Environ. 233, 111374 https://doi.org/10.1016/j.rse.2019.111374.

Zhu, Z., Piao, S., Myneni, R.B., Huang, M., Zeng, Z., Canadell, J.G., et al., 2016. Greening of the earth and its drivers. Nat. Clim. Chang. 6 (8), 791–795. https://doi.org/10.1038/nclimate3004.